



Neddylation modification of the U3 snoRNA-binding protein RRP9 by Smurf1 promotes tumorigenesis

Received for publication, April 7, 2021, and in revised form, September 29, 2021. Published, Papers in Press, October 15, 2021.
<https://doi.org/10.1016/j.jbc.2021.101307>

Meng-ge Du^{1,‡}, Fan Liu^{1,‡}, Yan Chang^{2,‡}, Shuai Tong¹, Wei Liu¹, Yu-jiao Chen¹, and Ping Xie^{1,*}

From the ¹Department of Cell Biology, The Municipal Key Laboratory for Liver Protection and Regulation of Regeneration, Capital Medical University, Beijing, China and ²Beijing Key Laboratory for Pediatric Diseases of Otolaryngology, Head and Neck Surgery, Key Laboratory of Major Diseases in Children, Ministry of Education, Beijing Pediatric Research Institute, Beijing Children's Hospital, Capital Medical University, National Center for Children's Health, Beijing, China

Edited by Ronald Wek

Neddylation is a posttranslational modification that attaches ubiquitin-like protein Nedd8 to protein targets *via* Nedd8-specific E1-E2-E3 enzymes and modulates many important biological processes. Nedd8 attaches to a lysine residue of a substrate, not for degradation, but for modulation of substrate activity. We previously identified the HECT-type ubiquitin ligase Smurf1, which controls diverse cellular processes, is activated by Nedd8 through covalent neddylation. Smurf1 functions as a thioester bond-type Nedd8 ligase to catalyze its own neddylation. Numerous ubiquitination substrates of Smurf1 have been identified, but the neddylation substrates of Smurf1 remain unknown. Here, we show that Smurf1 interacts with RRP9, a core component of the U3 snoRNP complex, which is involved in pre-rRNA processing. Our *in vivo* and *in vitro* neddylation modification assays show that RRP9 is conjugated with Nedd8. RRP9 neddylation is catalyzed by Smurf1 and removed by the NEDP1 deneddylase. We identified Lys221 as a major neddylation site on RRP9. Deficiency of RRP9 neddylation inhibits pre-rRNA processing and leads to downregulation of ribosomal biogenesis. Consequently, functional studies suggest that ectopic expression of RRP9 promotes tumor cell proliferation, colony formation, and cell migration, whereas unneddylated RRP9, K221R mutant has no such effect. Furthermore, in human colorectal cancer, elevated expression of RRP9 and Smurf1 correlates with cancer progression. These results reveal that Smurf1 plays a multifaceted role in pre-rRNA processing by catalyzing RRP9 neddylation and shed new light on the oncogenic role of RRP9.

Ribosome synthesis is highly conserved and regulated. It requires the coordinated cooperation of DNA-dependent RNA polymerases, transcription factors, small nucleolar ribonucleoproteins (snoRNPs), and ribosomal proteins (1–3). Ribosomes in eukaryotes are composed of a 40S small ribosomal subunit (containing 18S rRNA) and a 60S large ribosomal subunit (containing 5S rRNA, 5.8S rRNA, and 28S rRNA) (4). The initial 47S precursor ribosomal RNA (pre-rRNA) is

cleaved to form the mature 28S, 18S, and 5.8S rRNAs. Maturation of pre-rRNAs requires snoRNPs to undergo numerous posttranscriptional modifications. SnoRNAs are classified into seven categories, which are numbered U1–U7 due to their rich U content (5, 6). SnoRNAs exist only in the nucleus; U3 is present in nucleoli and is associated with the maturation of 18S rRNA in nucleoli, while the other six snoRNAs are present in the nucleoplasm and are associated with the splicing processing of precursor mRNAs (7, 8). U3 snoRNAs mainly interact with proteins containing a C/D frame structure to form U3 snoRNPs. Among those proteins, Nop1, Nop56, Nop58, and Snu13 are common to all C/D box snoRNAs, whereas RRP9, also called U3-55K, is a late cloned and identified member of the U3 snoRNA–protein complex. RRP9 is identified as a core subunit of the U3-snoRNP complex (9). To date, except for its acetylation, little is known about the posttranslational modification of RRP9 (10, 11).

Neuronal precursor cell expressed developmentally down-regulated 8 (Nedd8) is covalently conjugated to substrates in a manner similar to ubiquitin (12). Neddylation is a cascade of ATP-catalyzed enzymatic reactions mediated by an activating enzyme (E1, a heterologous dimer composed of UBA3 and NAE1/APP-BP1), two conjugating enzymes (E2s, UBE2M/Ubc12, and UBE2F) and a variety of E3 ligases (13). The covalently conjugated Nedd8 can be removed by deneddylases, including NEDP1 and JAB1/CSN5 (14, 15). The neddylation pathway is known to be overactivated in many tumors. MLN4924 and TAS4464, inhibitors of neddylation E1s, have been evaluated in a series of phase I/II/III clinical trials and have shown marked antitumor activity in diverse cancer models (16, 17). Therefore, neddylation has been indicated to be closely correlated with tumorigenesis (18–20). Nedd8 E3 ligases can be divided into two categories according to their structural characteristics: ring finger scaffold-type and HECT domain-type. Ring-type E3s include ROC1/RBX1, DCN1, MDM2, C-CBL, IAPs, RNF111, and RNF168 (21–28), which cannot form thioester bonds with Nedd8. The other types of HECT-type E3s include Smad ubiquitination regulatory factor 1 (Smurf1), RSP5, and ITCH (29, 30). Smurf1 functions as a thioester bond-type Nedd8 ligase to catalyze its own neddylation. Smurf1, Nedd8, NAE1, and Ubc12 are positively

[‡] These authors contributed equally to this work.

* For correspondence: Ping Xie, xiep@cmmu.edu.cn.

Smurf1 catalyzes RRP9 neddylation to promote tumorigenesis

correlated with progression and poor prognosis in human colorectal cancer (29). Although numerous ubiquitination substrates of Smurf1, such as Smad1/5/8, MEKK2, and RhoA (31–34), have been identified, its neddylation substrates remain unknown.

In this study, RRP9 was identified as a neddylation substrate of Smurf1. RRP9 neddylation promotes pre-rRNA processing, resulting in promotion of cell proliferation. Smurf1 deletion decreases the efficiency of pre-rRNA processing, and this effect is reversed by reintroduction of wild-type RRP9 but not its neddylation-depleted K221R mutant. Therefore, RRP9 neddylation mediated by Smurf1 has an important function in pre-rRNA synthesis. Furthermore, increased expression of Smurf1 and RRP9 shows a positive correlation with human colon cancer progression. These findings characterize the functional diversity of neddylation and reveal a new mechanism of Smurf1 in tumorigenesis.

Results

RRP9 interacts with Smurf1

High-throughput mapping of the dynamic TGF- β signaling network identified a series of potential Smurf1-interacting proteins, among which RRP9 was included (35). To further support the interaction, affinity purification and mass spectrometry were first employed to investigate the Smurf1 interactome. Whole-cell extracts were prepared and subjected to affinity purification on an anti-Smurf1 affinity gel. Mass spectrometry analysis indicated that Smurf1 was copurified with RRP9 (Figs. 1A and S1A). Endogenous RRP9 was efficiently coimmunoprecipitated with Smurf1 (Figs. 1B and S1B). Smurf1 was shown to interact with endogenous RRP9 (Fig. 1C). The glutathione S-transferase pull-down assay indicated that the interaction between RRP9 and Smurf1 seemed to be direct (Fig. 1D). In addition, Smurf1 colocalized with RRP9 in the nuclei of HCT116 cells (Fig. 1E). Then, full-length Myc-tagged RRP9 and the 1 to 144 aa and 145 to 475 aa truncations were transfected into HCT116 cells. Immunoprecipitation with an antibody against Myc-tagged proteins followed by immunoblotting with antibodies against Smurf1 showed that Smurf1 was efficiently coimmunoprecipitated with the WD40 domain (aa 145–475) of RRP9. (Fig. 1, G and H). Collectively, these data indicated that RRP9 was a Smurf1-specific interacting partner.

Smurf1 mediates RRP9 neddylation

Considering that Smurf1 is an E3 ligase for both ubiquitin and Nedd8, we first intended to investigate whether RRP9 can be ubiquitinated by Smurf1. MG132, a proteasome inhibitor, did not affect the protein stability of RRP9 compared with that of Smurf1 (Fig. 2A). In addition, knockout of Smurf1 did not affect the protein stability of RRP9 in HCT116 cells or mice (Fig. 2, B and C). The C426A mutation abolishes the catalytic activity of the Smurf1 neddylation ligase (29). Thus, we intended to detect the expression of RRP9 in *Smurf1*^{-/-} and *Smurf1*^{C426A} knock-in (KI) mice. The data showed that the protein level of RRP9 in *Smurf1*^{-/-} and *Smurf1*^{C426A} KI mice

did not differ from that in *Smurf1*^{+/+} mice (Fig. S2A), and the same result was found for its mRNA level (Fig. S2B). These data strongly indicated that Smurf1 does not affect the protein stability of RRP9 *via* the ubiquitin–proteasome pathway.

Next, we investigated whether RRP9 can be neddylated by Smurf1. To date, RRP9 neddylation has not been reported in the literature. To further evaluate this modification, immunoprecipitation (IP) under partial denaturing conditions was performed with an anti-RRP9 antibody in HCT116 cells, and the precipitates were detected as smeared bands. The densities of the smeared bands were clearly reduced by treatment with the E1 inhibitor MLN4924 (Fig. 2D). When Nedd8 was ectopically expressed, RRP9 migrated as a high-molecular-weight band, but the smeared bands were not produced from the lysate of cells expressing Nedd8- Δ GG, a mutant incapable of covalent conjugation to its substrates (Fig. 2E), suggesting that the smeared bands correspond to Nedd8-conjugated RRP9. Moreover, knockout of NEDP1 by sgRNA increased RRP9 neddylation (Fig. 2F), which indicated that NEDP1 is the deneddylase for RRP9. These data suggested that RRP9 was conjugated with Nedd8.

We next determined whether Smurf1 is involved in RRP9 neddylation. Immunoprecipitation under partial denaturing conditions was performed with an anti-RRP9 antibody, and the precipitates were analyzed. The results revealed that endogenous RRP9 was covalently conjugated to Nedd8 but not ubiquitin in the colon tissues of *Smurf1*^{+/+} mice (Fig. 2G, Lane 2; Fig. 2H, Lane 2). We found that RRP9 neddylation was almost completely abolished in *Smurf1*^{-/-} and *Smurf1*^{C426A} KI mice (Fig. 2G, Lane 3; Fig. 2H, Lane 3). In addition, RRP9 neddylation was markedly reduced with deletion of UBA3 (neddylation E1), Ubc12 (neddylation E2), and Smurf1 using target sgRNAs (Fig. 2I). In addition, ectopic expression of Smurf1 markedly enhanced the neddylation of RRP9 (Fig. 2J). Finally, *in vitro* neddylation assays were performed with purified RRP9, Smurf1, Nedd8, NAE (E1), and Ubc12 (E2). The results showed that Smurf1 catalyzed RRP9 neddylation *in vitro* (Fig. 2K). Collectively, these data supported the hypothesis that Smurf1 is likely the major Nedd8 E3 ligase for RRP9.

Smurf1 catalyzes RRP9 neddylation at K221

Analysis of the RRP9 sequence showed that it contained a total of 29 lysines: 7 lysines in the N-terminal domain, 8 lysines in the Glu-rich region, 13 lysines in the WD40 domain, and 1 lysine in the C-terminal domain (Fig. 3A). We generated RRP9 truncations to identify the neddylation regions in RRP9. The results in HCT116 cells showed that the 1 to 144 aa region in RRP9 could not be neddylated, indicating that these 15 lysines were not RRP9 neddylation sites (Fig. 3B). Then, individual K-R mutations in the region from 145 aa to 475 aa, which contains 14 lysines in RRP9, were introduced to identify the sites of Nedd8 covalent conjugation. The K221R mutant exhibited almost no neddylation compared with the other K-R mutants (Fig. 3C). Further *in vitro* neddylation assays confirmed that Smurf1 could not catalyze RRP9 K221R neddylation (Fig. 3D).

Smurf1 catalyzes RRP9 neddylation to promote tumorigenesis

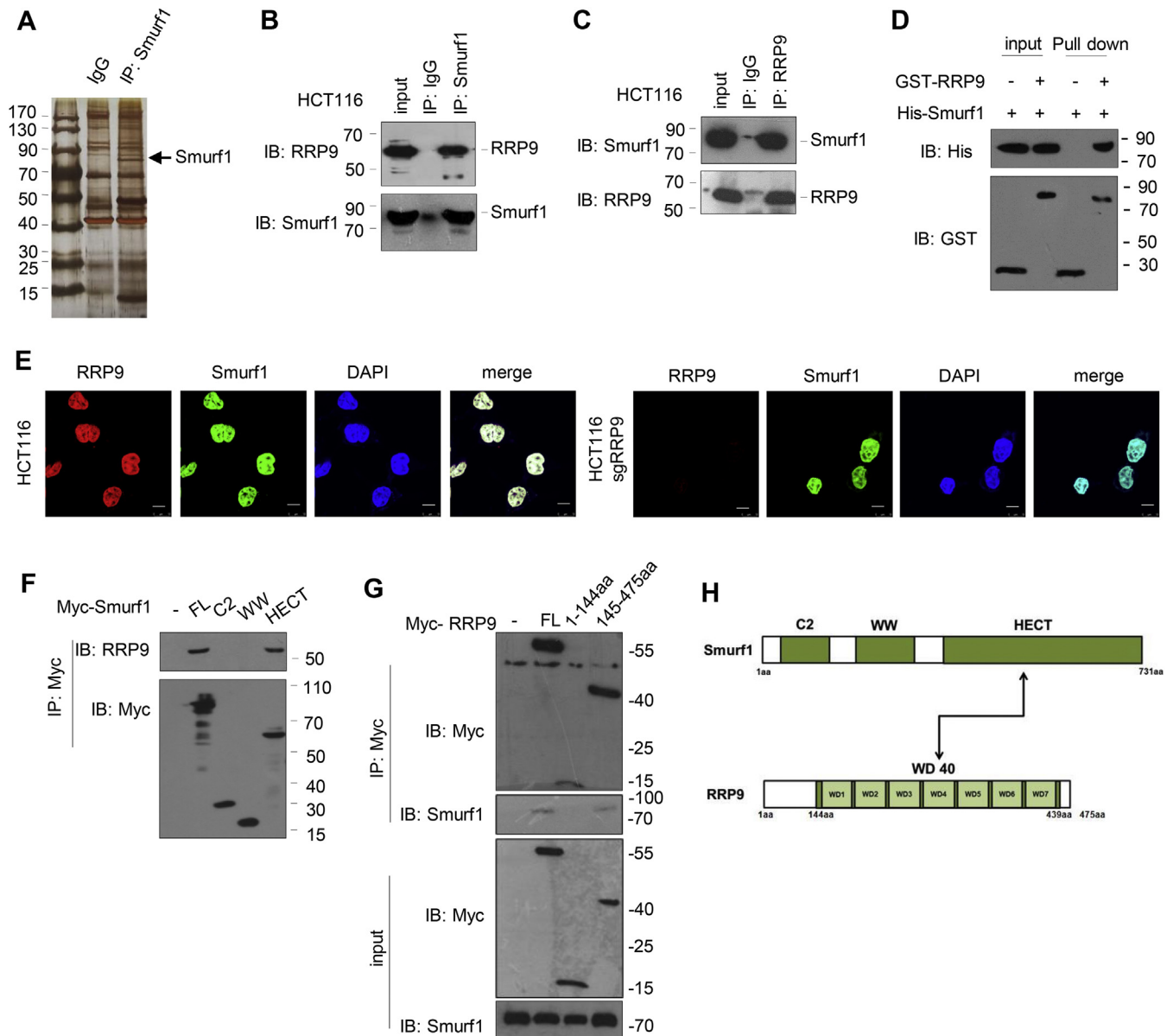


Figure 1. Smurf1 interacts with RRP9. *A* and *B*, cellular extract from HCT116 cells was immunopurified with anti-Smurf1 antibody (ab117552) and then eluted. The eluates were resolved by SDS-PAGE and silver-stained. The protein bands were retrieved and analyzed by mass spectrometry. Immunopurified proteins were analyzed by western blotting using antibodies against the indicated proteins. *C*, immunoblot of anti-RRP9 immunoprecipitate from HCT116 cells. *D*, GST pull-down assays of His-Smurf1 with GST or GST-RRP9 are indicated. *E*, immunofluorescence of RRP9 and Smurf1 is indicated in HCT116 cells. Scale bar, 25 μ m. *F-H*, mapping the interaction binding regions between RRP9 and Smurf1. Shown is mapping the RRP9 binding region on Smurf1. Cell lysates from HCT116 cells transfected with Myc-tagged Smurf1 or Myc-tagged RRP9 deletion mutants were immunoprecipitated with anti-Myc followed by immunoblotting with anti-RRP9 or anti-Smurf1.

Therefore, these data suggested that K221 was the major site of RRP9 neddylation.

Loss of RRP9 inhibits tumorigenesis

The role of RRP9 in tumor prognosis remains unknown. Next, we explored the role of RRP9 in tumorigenesis. We generated stably transduced HCT116 colon cancer cells by performing lentiviral transduction with Lenti-sgNC (negative control) and Lenti-sgRRP9 (Fig. S3A). The CCK-8 and colony formation assay results indicated that deletion of RRP9 notably inhibited cell proliferation (Fig. 4, A and B). Knockout of RRP9

decreased tumor cell migration (Fig. 4C). Then, we intended to determine whether RRP9 affects cellular senescence in tumors. SA- β -Gal staining showed that deletion of RRP9 increased tumor cell senescence (Fig. 4D). Furthermore, loss of RRP9 obviously inhibited tumor growth in xenografted nude mice (Fig. 4, E-G). Consistent with previous findings, knockout of RRP9 led to a reduction in the total 18S rRNA level (Fig. 4H). Ribosome assembly is coupled with irreversible pre-rRNA processing, which is a classical hallmark of cell growth and proliferation. Therefore, interference with ribosomal biogenesis is often associated with cancer. RRP9 is reported to be essential for U3 snoRNP assembly and ribosomal RNA maturation

Smurf1 catalyzes RRP9 neddylation to promote tumorigenesis

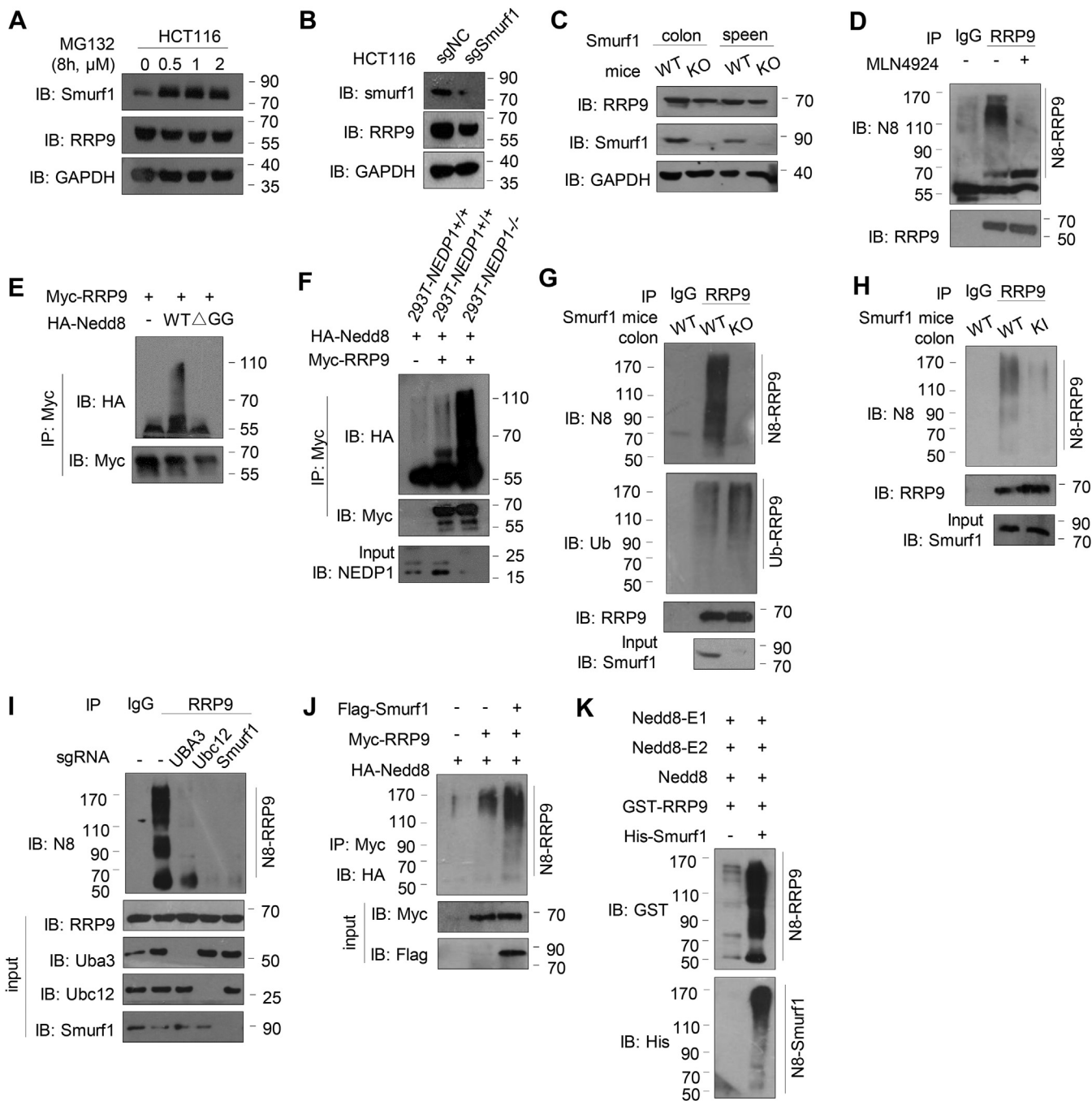


Figure 2. Smurf1 serves as an E3 ligase of RRP9 neddylation. *A*, HCT116 cells were treated with MG132 (0, 0.5, 1, 2 μ M) for 8 h. Immunoblot analysis of whole cell lysates (WCL) from HCT116 cells. *B*, immunoblot of WCL from *Smurf1*-deleted HCT116 cells. *C*, immunoblot analysis of indicated proteins from the tissues of *Smurf1*-WT or *Smurf1*-KO mice. *D*, RRP9 neddylation was attenuated by MLN4924 (1 μ M, 16 h). Immunoblot analysis of anti-RRP9 immunoprecipitate and WCL from HCT116 cells. *E*, immunoblot of anti-Myc immunoprecipitate and WCL from HCT116 cells transfected with indicated constructs. *F*, RRP9 neddylation was enhanced by the deletion of *NEDP1*. Immunoblot analysis of anti-Myc tagged RRP9 immunoprecipitate and WCL from HEK293T *NEDP1*^{+/+} and *NEDP1*^{-/-} cells. *G* and *H*, RRP9 neddylation was reduced in *Smurf1*^{-/-} (KO) or *Smurf1*^{C426A} (KI) mice. Immunoblot analysis of anti-RRP9 immunoprecipitate and WCL from the tissues of *Smurf1* WT, KO or KI mice. *I*, RRP9 neddylation was attenuated by deletion of UBA3, Ubc12, Smurf1. Immunoblot analysis of anti-RRP9 immunoprecipitate and WCL from HCT116 cells. *J*, overexpression Smurf1 increases RRP9 neddylation. Immunoblot of anti-Myc immunoprecipitate and WCL from HCT116 cells transfected with indicated constructs. *K*, *in vitro* covalent neddylation of RRP9. Purified His-Smurf1 and GST-RRP9 proteins were incubated with Nedd8, Nedd8-E1/E2. Reactions were performed as described in the Methods section. Samples were analyzed by western blotting with indicated antibody.

(36, 37). Enlarged nucleoli are typically associated with activation of ribosome biogenesis. Silver staining was used for the identification of argyrophilic nucleolar organizer regions (AgNORs). RRP9 knockout resulted in a lower average AgNOR

area of positive silver staining. This suggested that knockout of RRP9 leads to downregulation of ribosomal biogenesis (Fig. 4J). Collectively, the aforementioned data suggested that loss of RRP9 inhibited tumor cell growth and migration.

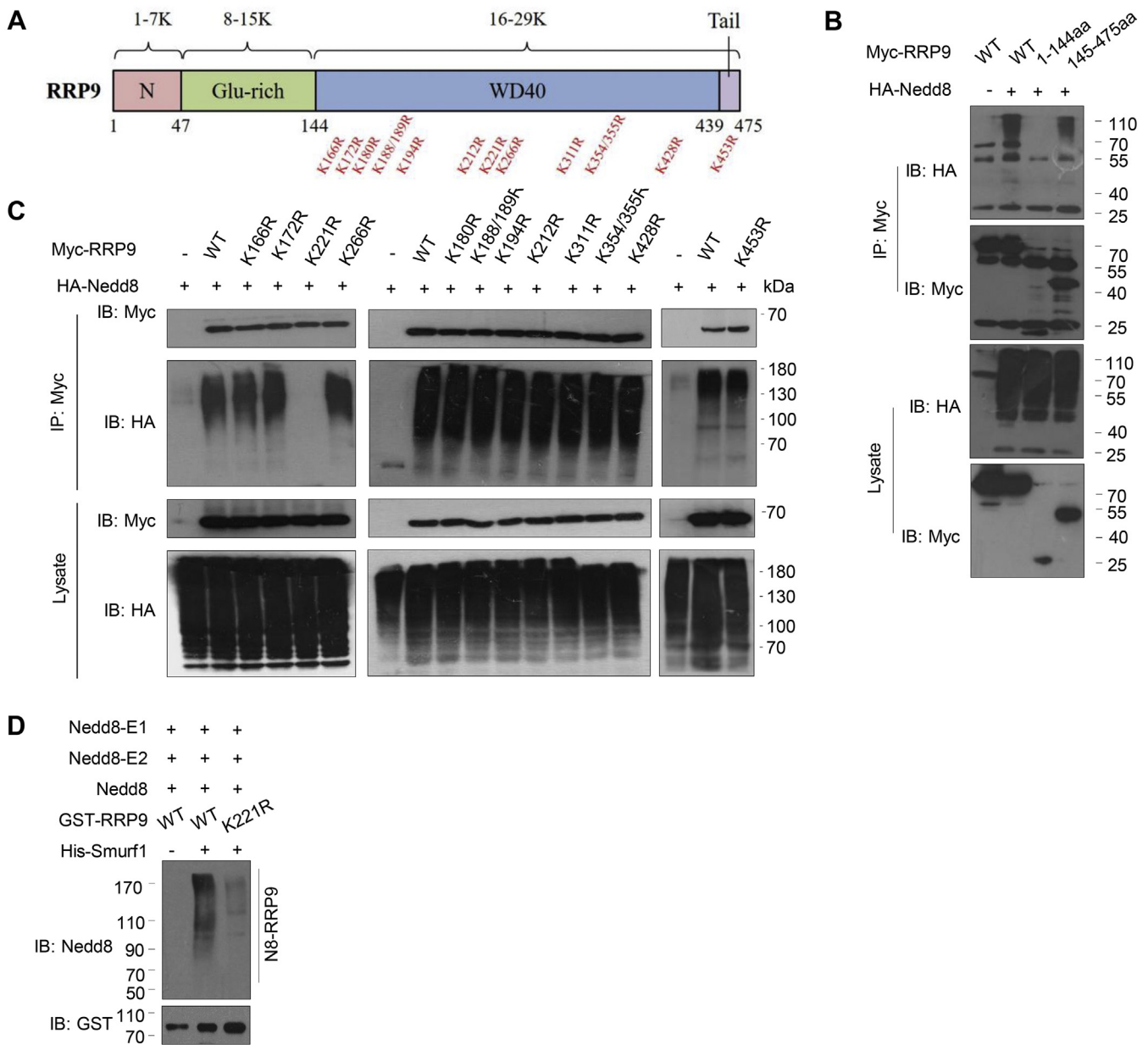


Figure 3. Smurf1 promotes RRP9 neddylation on K221. *A*, a schematic diagram of the lysine sites on RRP9 is shown. *B*, *in vivo* RRP9 neddylation assay. Immunoblot analysis of anti-Myc immunoprecipitate and WCL from HCT116 cells transfected with indicated constructs. *C*, RRP9 neddylation occurred on K221. Immunoblot analysis of anti-Myc immunoprecipitate and WCL from HCT116 transfected with indicated constructs. *D*, purified His-Smurf1 and GST-RRP9 WT or K221R proteins were incubated with Nedd8, Nedd8-E1/E2. Reactions were performed and analyzed by western blotting.

RRP9 neddylation promotes pre-rRNA processing and tumorigenesis

To gain insight into the role of RRP9 neddylation in cancer progression, we reintroduced sgRNA-resistant RRP9-WT and K221R into HCT116 cells with RRP9 deletion (Fig. S3B). Then, RNA was labeled with biotin and analyzed by fluorography. Consistent with previous findings, the data revealed that the amount of 18S rRNA was reduced in RRP9-knockout cells (Fig. 5A, Lane 2). Notably, reintroduction of wild-type RRP9 rescued this effect, whereas reintroduction of the neddylation-deficient mutant of RRP9 (K221R) did not restore processing (Fig. 5A, Lanes 3 and 4). Next, AgNORs were identified to evaluate alterations in nucleolar morphology. Silver staining showed

that RRP9 knockout resulted in a reduction in the average AgNOR area, while ectopic expression of RRP9-WT markedly reversed these effects. RRP9-K221R overexpression had no such effect (Fig. 5B). This suggested that RRP9 neddylation leads to upregulation of ribosomal biogenesis. Considering that elevated ribosomal biogenesis is typically associated with stimulation of cell proliferation (38, 39), we then investigated tumor cell proliferation changes resulting from RRP9 neddylation. The growth curves showed a reduced cell growth rate resulting from RRP9 deletion (Fig. 5, C and D). Reintroduction of RRP9-WT significantly promoted cell proliferation. In contrast, reintroduction of RRP9-K221R into these cells caused a nonsignificant increase in tumor growth (Fig. 5, C and D). Moreover, ectopic expression of

Smurf1 catalyzes RRP9 neddylation to promote tumorigenesis

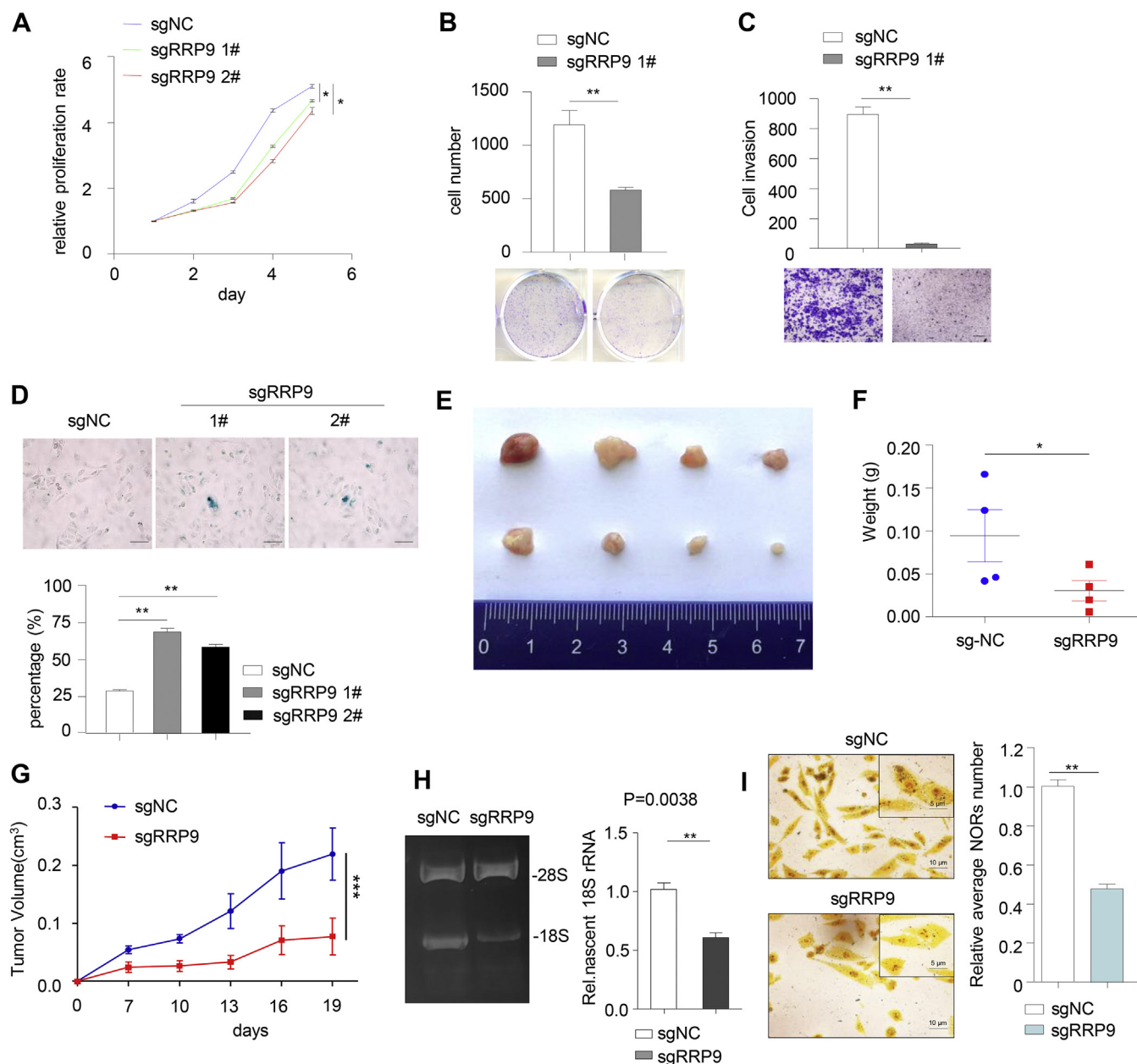


Figure 4. Knockout of RRP9 inhibits tumorigenesis. A–C, CCK8 assay (A), colony formation assay (B), and cell migration assay (C) were performed in the indicated cells. Data are presented as the mean \pm S.D. Results are from a representative experiment performed in triplicate. Image J was used to perform quantitative analysis. D, β -galactosidase (β -gal) assay were performed in the indicated cells. Image J was used to perform quantitative analysis. The differences between groups were assessed by one-way ANOVA test. E–G, nude mice were injected subcutaneously for each of the indicated stable cell lines. The transplanted tumors were removed and photographed (E). Tumors were isolated, weights (F) and their volumes were measured (G). H, 28S and 18S rRNA levels in RRP9 knockout cells. Total RNA was extracted from wild-type HCT116 cells and RRP9 knockout cells, followed by resolution on a 1% formaldehyde-agarose gel for comparison. I, average area of nucleolar organizing regions in RRP9 knockout cells. Left panel, images of silver staining. Right panel, quantitative analysis of AgNOR indices. AgNOR from 20 cells was measured in each group. The scale bars represent 10 μ m. Data are shown as the mean \pm S.D. *p* values were calculated by Student's *t* test (B, C, F, H, and I), one-way ANOVA test (A and D), and two-way ANOVA test (G). **p* < 0.05, ***p* < 0.01, ****p* < 0.001.

RRP9 markedly enhanced tumor cell migration, but over-expression of RRP9-K221R had no such effect (Fig. 5E). Collectively, these data indicated that RRP9 neddylation promoted pre-rRNA processing and activation of ribosomal biogenesis, which resulted in enhanced tumor cell proliferation and migration.

Smurf1 promotes pre-rRNA processing

If Smurf1-mediated RRP9 neddylation is required for proper 18S rRNA processing, depletion of either RRP9 or Smurf1

should cause similar defects in pre-rRNA processing. In fact, the function of Smurf1 in pre-rRNA synthesis remains unknown. We generated a cell line with stable deletion of Smurf1 to investigate pre-rRNA synthesis (Fig. 6A). Fluorographic analysis indicated that the amount of 18S rRNA was reduced in Smurf1-knockout cells (Fig. 6, B–D). Total RNA was extracted and resolved on a 1% formaldehyde-agarose gel. These results also showed that knockout of RRP9 led to a decrease in the total 18S rRNA abundance (Fig. S3C). Furthermore, Smurf1 knockout resulted in a decrease in

Smurf1 catalyzes RRP9 neddylation to promote tumorigenesis

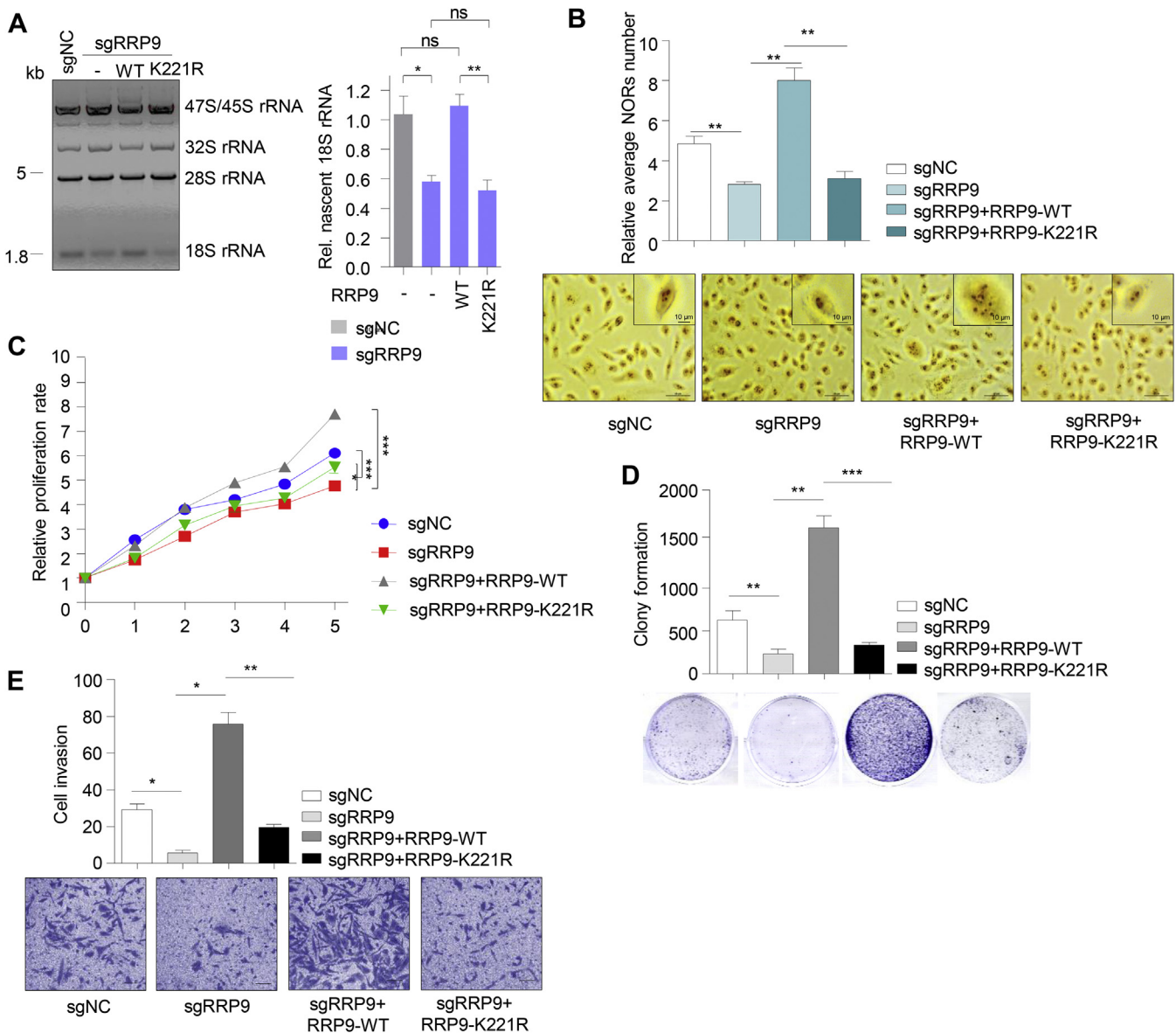


Figure 5. Neddylated RRP9 is required for tumorigenesis. A, RRP9 WT or K221R mutant vectors were each stably transfected into HCT116 cells that were depleted of RRP9 using a Lentivirus-coupled shRNA against RRP9. RNA was labeled with biotin-16-UTP and analyzed by fluorography. Bars represent means of radio-labeled 18S rRNA \pm S.D. from three experiments. B, average area of nucleolar organizing regions in indicated cells. *Up panel*, quantitative analysis of AgNOR indices. *Down panel*, images of silver staining. AgNOR from 20 cells was measured in each group. The scale bars represent 50 μ m. C and E, CCK8 assay (C), colony formation assay (D), and cell migration assay (E) were performed in the indicated cells. Data are presented as means \pm S.D. Results are from a representative experiment performed in triplicate. Image J was used to perform quantitative analysis. *p* values were calculated by one-way ANOVA test (A, B, D, and E) and two-way ANOVA test (C). **p* < 0.05, ***p* < 0.01, ****p* < 0.001.

nucleoli (Fig. 6E). Therefore, it was concluded that deletion of Smurf1 inhibited pre-rRNA processing.

Smurf1 plays an oncogenic role in colon cancer (29). We intended to explore whether Smurf1 promotes tumorigenesis by regulating pre-rRNA processing. Consistent with previous findings, Smurf1 knockout resulted in marked decreases in the tumor cell growth rate (Fig. 6, F and G) and cell migration (Fig. 6H), and Smurf1-knockout cells displayed indications of severe senescence defects (Fig. 6I). Next, sgSmurf1-cotransfected RRP9-WT and RRP9-K221R cell lines were generated (Fig. S3D). Silver staining showed that Smurf1 knockout resulted in a reduction in the average AgNOR area.

Ectopic expression of RRP9-WT markedly reversed these effects, but overexpression of RRP9-K221R had almost no effect (Fig. 6J), indicating that neddylation of RRP9 might be important but not essential for Smurf1 to accelerate pre-rRNA processing. Moreover, deletion of Smurf1 markedly suppressed cell proliferation, colony formation, and cell migration, whereas introduction of wild-type RRP9 rescued the processing defect (Fig. 6, K–M). However, introduction of the neddylation-deficient mutant of RRP9 (K221R) did not restore processing (Fig. 6, K–M). These data demonstrated that the oncogenic role of Smurf1 was involved in the positive regulation of pre-rRNA synthesis by catalyzing RRP9 neddylation.

Smurf1 catalyzes RRP9 neddylation to promote tumorigenesis

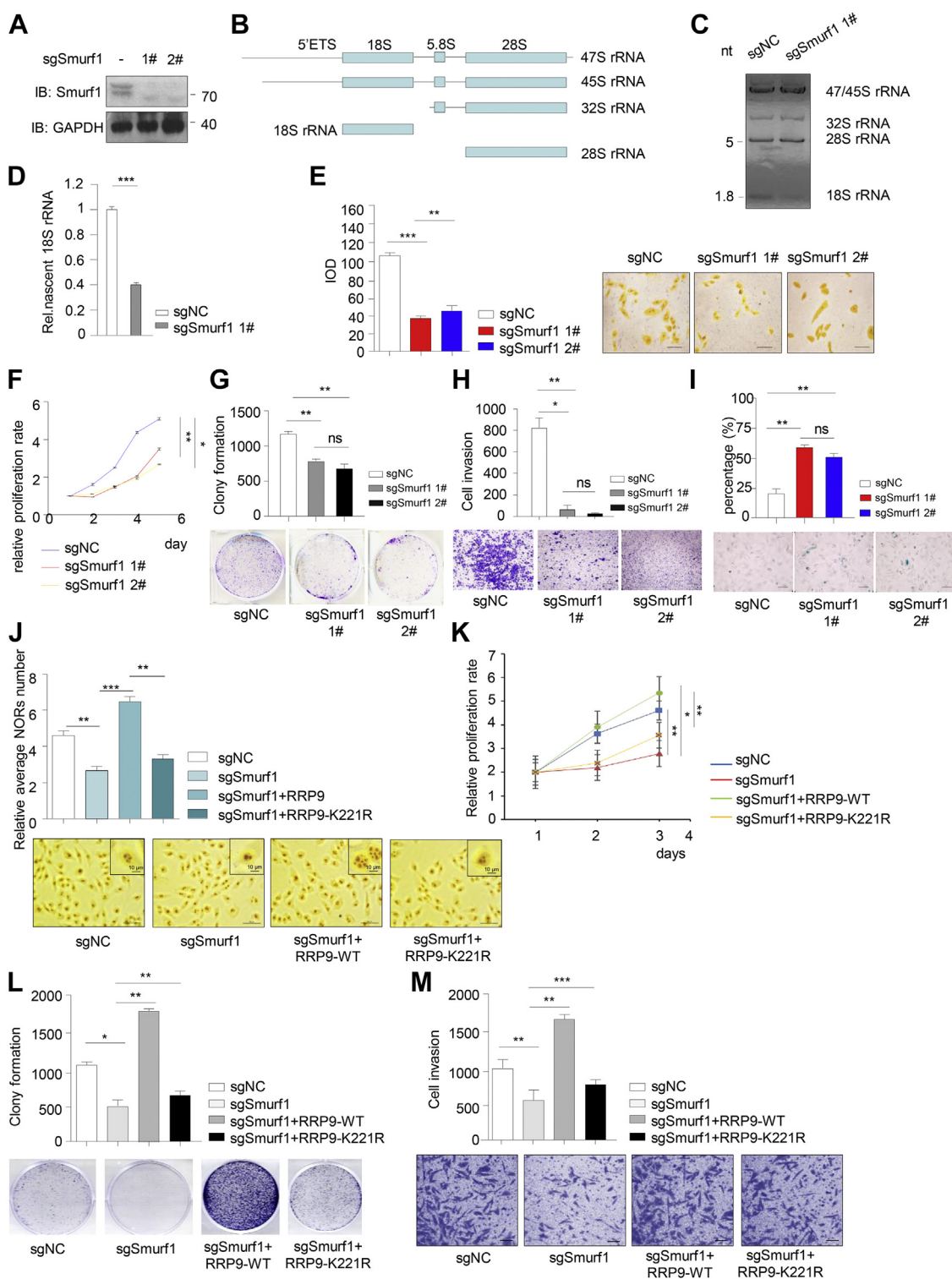


Figure 6. Smurf1 neddylation of RRP9 to promote tumorigenesis. *A*, Smurf1 was deleted by lentivirus-coupled sgRNA. The expression of Smurf1 was detected by western blot to determine the efficiency of deletion. *B–D*, RNA was labeled with biotin and analyzed by fluorography in Smurf1 knockout cells. Bars represent means of radio labelled 18S rRNA \pm S.D. from three experiments. *E*, average area of nucleolar organizing regions in indicated cells. *Left panel*, quantitative analysis of AgNOR indices. *Right panel*, images of silver staining. AgNOR from 20 cells was measured in each group. The scale bars represent 50 μ m. *F–H*, CCK8 assay (*F*), colony formation assay (*G*), and cell migration assay (*H*) were performed in the indicated cells. Data are presented as means \pm S.D. Results are from a representative experiment performed in triplicate. Image *J* was used to perform quantitative analysis. The differences between groups were assessed by one-way ANOVA test. *p* values were calculated by one-way ANOVA test (*E*, *G*, *H*, and *I*) and two-way ANOVA test (*F*). **p* < 0.05, ***p* < 0.01, ****p* < 0.001. *J*, average area of nucleolar organizing regions in indicated cells. *Up panel*, quantitative analysis of AgNOR indices. *Down panel*, images of silver staining. AgNOR from 20 cells was measured in each group. The scale bars represent 50 μ m. *K–M*, CCK8 assay (*K*), colony formation assay (*L*), and cell migration assay (*M*) were performed in the indicated cells. Data are presented as means \pm S.D. Results are from a representative experiment performed in triplicate. Image *J* was used to perform quantitative analysis. *p* values were calculated by one-way ANOVA test (*J*, *L*, and *M*) and two-way ANOVA test (*K*). **p* < 0.05, ***p* < 0.01, ****p* < 0.001.

RRP9 positively correlates with Smurf1 in colon cancer

Previous data indicated that Nedd8-mediated Smurf1 activation promotes colon cancer progression (29). Human colorectal cancer tissue samples and matched adjacent normal tissue samples were evaluated to investigate the potential clinical relevance of RRP9 in colon cancer. Compared with that in distal and adjacent tissues, RRP9 expression was notably increased in tumor tissues (Fig. 7, A and B). The samples were divided into groups based on the tumor stage to better understand the correlation of RRP9 with colon cancer progression. The results showed that the expression of RRP9 was lower in low-TNM stage tumors and higher in high-TNM stage tumors (Fig. 7, C and D). Consistent with previous findings, these results also indicated that Smurf1 was significantly upregulated in colorectal cancer tissues compared with matched adjacent tissues (Fig. 7, E and F), in addition to the high expression of RRP9 in tumor tissues (Fig. 7, E and G). Importantly, a positive correlation of Smurf1 with RRP9 was observed among patients with tumors (Fig. 7H). Both the expression and neddylation of RRP9 were clearly upregulated in patients with colorectal cancer (Fig. 7, I–K). Taken together, these data suggested that RRP9 was highly expressed in colon cancer, concomitant with the enhancement of Smurf1-catalyzed RRP9 neddylation, to promote tumor progression.

Discussion

Previous studies reported that Nedd8 ligases such as Dcn1, Roc1/Rbx1, IAPs, c-Cbl, RNF111, RNF168, and MDM2 are all RING finger scaffold-type E3s. Smurf1 is the first identified HECT-type Nedd8 ligase to supplement the classification of Nedd8 ligases. Smurf1 integrates the ubiquitination and neddylation pathways as a dual E3 ligase. Smurf1 forms a Nedd8-thioester intermediate and then catalyzes its own neddylation on multiple lysine residues. This neddylation enhances Smurf1-mediated ubiquitination (29, 40). A large number of Smurf1 ubiquitination substrates have been identified and include Smad1/5, MEKK2, and RhoA (31–33). The latest reports show that Smurf1 ubiquitinates and degrades PTEN in glioblastoma (41). PTEN has been suggested to be a neddylation substrate, and XIAP is the major Nedd8 E3 ligase for PTEN (42). Smurf1 promotes USP25 ubiquitination and degradation to restrict its antiviral function (43), and ubiquitination of UVRAG by Smurf1 enhances autophagosome maturation (44). A large number of ubiquitination substrates have been identified, but the neddylation substrates for which Smurf1 serves as a Nedd8 ligase remain unidentified. This study identified RRP9 as a potential substrate for Smurf1-catalyzed neddylation. RRP9 is an interacting protein of Smurf1, and the HECT domain of Smurf1 interacts with the WD40 domain of RRP9.

RRP9 associates with U3 snoRNA to promote the cleavage of pre-18S rRNA (45, 46). Despite the importance of RRP9 in pre-rRNA processing, the understanding of the mechanisms underlying pre-rRNA processing regulation is limited. Acetylation of RRP9 is mediated by PCAF, while it is deacetylated by SIRT7 (10, 11). Deacetylation enhances RRP9 binding to U3

snoRNA, which is required for pre-rRNA processing (11). For the rest of the posttranslational modifications, the functional regulation of RRP9 is unclear. Our results revealed that Nedd8 is covalently conjugated to RRP9 *in vivo* and that K221 is the neddylation site. NEDP1 serves as a deneddylase for RRP9. This study confirmed Smurf1 as a specific Nedd8 E3 ligase for RRP9 both *in vivo* and *in vitro*. RRP9 neddylation was almost completely abolished in *Smurf1*^{C426A} KI mice with loss of Smurf1 neddylation activity. Based on this evidence, it was concluded that Smurf1 serves as a ligase for RRP9 neddylation at K221.

This study also demonstrated that neddylation of RRP9 plays a crucial role in the progression of pre-rRNA synthesis. Smurf1 interacted with the WD repeats of RRP9, which was also the U3 snoRNA binding region of the RRP9 protein (47). Expression of unneddylatable RRP9 (the RRP9-K221R mutant) impaired pre-rRNA processing, which resulted in elevated ribosomal biogenesis and tumor cell proliferation. Interestingly, the data indicated that Smurf1 is involved in pre-rRNA processing. Deletion of Smurf1 markedly inhibited pre-rRNA processing and reduced the average areas of nucleoli. Moreover, RRP9 neddylation was important for Smurf1 to regulate pre-rRNA processing but was not essential. RRP9 has a neddylation-independent function, and further investigation is necessary. This study is novel in revealing that Smurf1 controls pre-rRNA processing to promote tumor cell proliferation. Finally, it also demonstrated that RRP9 neddylation is closely associated with tumorigenesis in colorectal cancer. The levels of RRP9 expression and RRP9 neddylation were both higher in cancer tissues than in matched adjacent tissues. RRP9 expression showed a positive correlation with Smurf1 expression in patients with colon cancer. This study is novel in illustrating the possible role of RRP9 in tumorigenesis.

Taken together, the data in this study define neddylation as a necessary modification of RRP9 and reveal a previously unidentified pre-rRNA synthesis-promoting role of Smurf1. These findings might deepen the understanding of neddylation functions and provide detailed insights into precision cancer therapies. Small-molecule inhibitors of RRP9 neddylation should be developed as novel anticancer agents in the future.

Experimental procedures

Antibodies, mouse, and reagents

All antibodies were purchased as follows: anti-Smurf1 (ab117552, Abcam; SC-100616, Santa Cruz Biotechnology), anti-Ubc12 (ab56383, Abcam), anti-RRP9 (ab168845, Abcam), anti-Nedd8 (ALX-210-194-R200, Alexis Biochemicals), anti-Uba3 (ab247153, Abcam), anti-ubiquitin (ab134953, Abcam), anti-NEDP1 (ab229093, Abcam), anti-Myc (M192, MBL), anti-GST (PM013, MBL), anti-His (D291, MBL), anti-GAPDH (M171, MBL), anti-Flag (M185, MBL). The *Smurf1*^{-/-} and *Smurf1*^{C426A} mice were generated by Nanjing Biomedical Research Institute of Nanjing University. All mice were maintained and handled in accordance with protocols approved by the Capital Medical University. Routine genotyping primers were listed in Table S1. The NAE inhibitor

Smurf1 catalyzes RRP9 neddylation to promote tumorigenesis

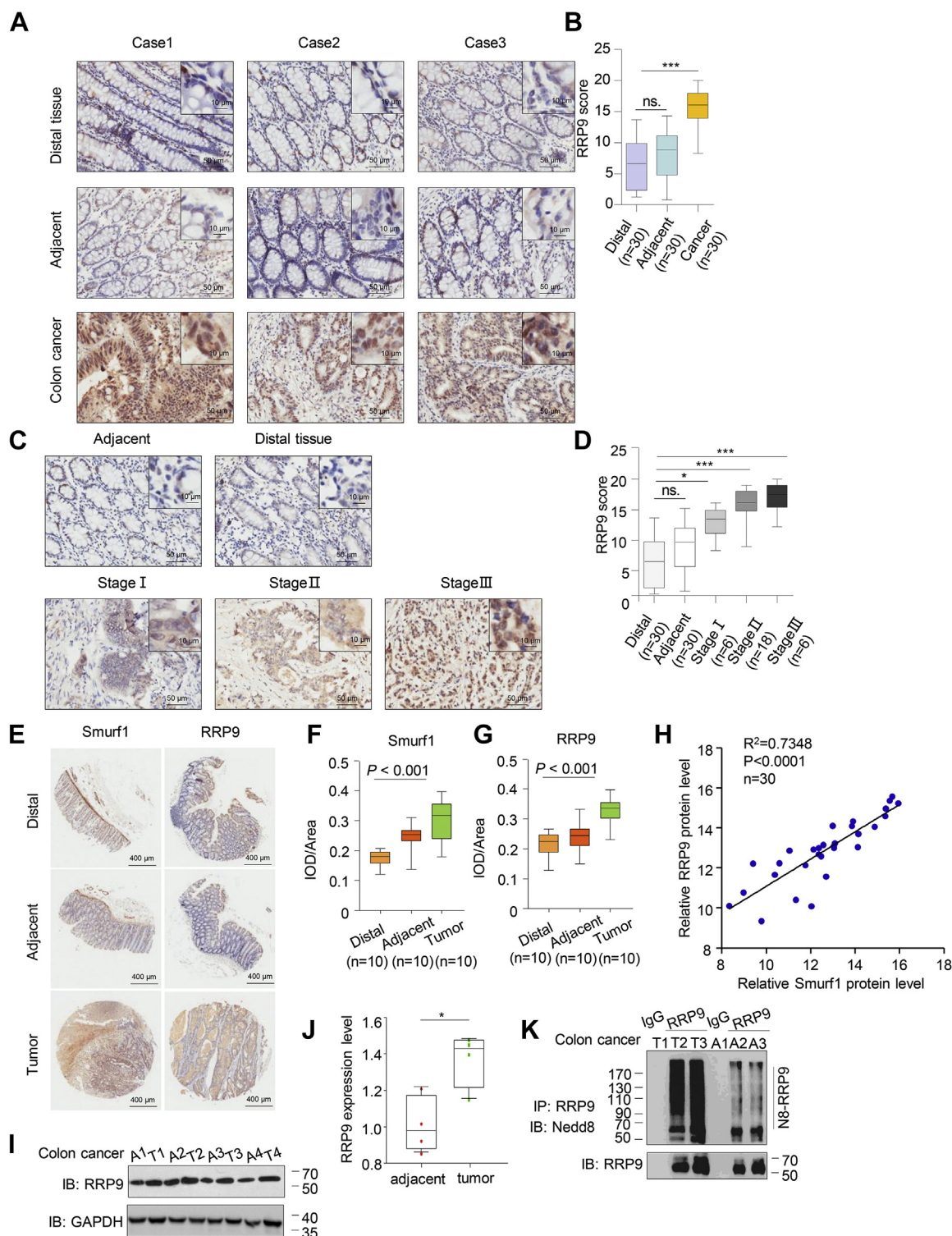


Figure 7. Positive correlation of RRP9 with Smurf1 in colon cancer. A, representative image from immunohistochemical staining of RRP9 in tumors and matched adjacent tissue. Image J was used to perform semiquantitative analysis. Scale bars, 50 μ m. B, RRP9 expression scores are shown as box plots. Data were analyzed using the Kruskal–Wallis test. C, representative images from immunohistochemical staining of RRP9 in two serial sections of the same tumor in different stages are shown. Scale bars, 50 μ m. D, box plot of RRP9 in tumors with different stages. Data were analyzed using the Kruskal–Wallis test. Image J was used to perform semiquantitative analysis. E, representative image from immunohistochemical staining of RRP9 and Smurf1 in tumors and matched adjacent tissue. Image J was used to perform semiquantitative analysis. Scale bars, 10 μ m. F and G, Smurf1 (F) and RRP9 (G) expression scores are shown as box plots. Data were analyzed using the Kruskal–Wallis test. H, positive correlation of RRP9 with Smurf1. Data were calculated by both Chi-Square and Mann–Whitney tests. Image J was used to perform semiquantitative analysis. I and J, RRP9 was higher in colon tumor patients. Immunoblot analysis of anti-RRP9 immunoprecipitate from adjacent and colon cancer tissues. RRP9 expression scores are shown as box plots. Data were analyzed using the Kruskal–Wallis test. K, RRP9 neddylation was higher in colon tumor patients. Immunoblot analysis of anti-RRP9 immunoprecipitate from adjacent and colon cancer tissues. p values were calculated by one-way ANOVA test (B, D, F, and G) and log-rank test (H). *** $p < 0.001$. A, adjacent tissue; T, tumor tissue.

Smurf1 catalyzes RRP9 neddylation to promote tumorigenesis

MLN4924 (HY-70062), proteasome inhibitor MG132 (HY-13259) were purchased from MCE.

Cell culture and transfections

HCT116, HT29, HEK293T were purchased from ATCC and authenticated by STR profiling and tested for *mycoplasma* contamination by GENEWIZ. HEK293T *NEDP1*^{+/+} and *NEDP1*^{-/-} cells were kindly gifted by Professor Xiaofeng Zheng from Peking University. The cells were cultured in DMEM medium supplemented with 10% fetal bovine serum (FBS). Cells were transfected with various plasmids using Sage LipoPlus™, Lipofectamine 3000 (Invitrogen, L3000001) according to the manufacturer's protocol.

LC-MS/MS analysis

Proteins in IP samples were precipitated with IP buffer (0.5% NP-40, 50 mM Tris, pH 7.6, 120 mM NaCl, 1 mM EDTA, 1 mM Na₃VO₄, 50 mM NaF, and 1 mM β-mercaptoethanol) and then washed three times with IP buffer. The samples from in-gel digestion were analyzed on a Thermo Q Exactive (Thermo Fisher Scientific) interfaced with an EASY-nLC 1000 UPLC system (Thermo Fisher Scientific). The tryptic peptides were dissolved in 0.1% FA, directly loaded onto a reversed-phase precolumn (Acclaim PepMap 100, Thermo). Peptide separation was performed using a reversed-phase analytical column (Acclaim PepMap RSLC, Thermo). The gradient was comprised of an increase from 6% to 25% solvent B (0.1% FA in 98% ACN) over 16 min, from 25% to 40% over 6 min, and climbing to 80% in 4 min then holding at 80% for the last 4 min, all at a constant flow rate of 320 nl/min on an EASY-nLC 1000 UPLC system. The peptides were subjected to NSI source followed by tandem mass spectrometry (MS/MS) in Q Exactive™ (Thermo) coupled online to the UPLC. Intact peptides were detected in the orbitrap at a resolution of 70,000. Peptides were selected for MS/MS using NCE setting as 28; ion fragments were detected in the orbitrap at a resolution of 17,500. A data-dependent procedure that alternated between one MS scan followed by 20 MS/MS scans was applied for the top 20 precursor ions above a threshold ion count of 5E3 in the MS survey scan with 15.0 s dynamic exclusion. The electrospray voltage applied was 2.0 kV. Automatic gain control (AGC) was used to prevent overfilling of the orbitrap; 5E4 ions were accumulated for generation of MS/MS spectra. For MS scans, the m/z scan range was 350 to 1800. The resulting MS/MS data were processed using Mascot search engine (v.2.3.0). Tandem mass spectra were searched against Swissport *Human* database. Trypsin/P was specified as cleavage enzyme allowing up to two missing cleavages. Mass error was set to 10 ppm for precursor ions and 0.02 Da for fragment ions. Carbamidomethyl on Cys was specified as fixed modification, and oxidation on Met, acetylation on Protein N-term were specified as variable modifications. Peptide ion score was set ≥20. Protein identification data (accession numbers, peptides observed, sequence coverage) are available in Table S2. All raw data and search results have been

deposited to the PRIDE database (<http://www.iprox.org/index>). The accession number is PXD024476.

Immunoprecipitation and immunoblotting

For immunoprecipitation assays, cells were lysed in EBC lysis buffer (0.5% NP-40, 50 mM Tris, pH 7.6, 120 mM NaCl, 1 mM EDTA, 1 mM Na₃VO₄, 50 mM NaF, and 1 mM β-mercaptoethanol) supplemented with protease inhibitor cocktail (Roche, 11836170001). Immunoprecipitations were performed using the indicated primary antibody and protein A/G agarose beads (Santa Cruz, sc-2003) at 4 °C. The immunoprecipitants were washed at least three times in NETN lysis buffer (150 mM NaCl, 1 mM EDTA, 50 mM Tris-HCl, pH7.8, 1% NP-40, 1 mM phenylmethylsulfonyl fluoride) before being resolved by SDS-PAGE and immunoblotted with indicated antibodies.

GST pull-down assay

Bacteria-expressed GST-tagged proteins were immobilized on glutathione Sepharose 4B beads (Amersham Biosciences) and then incubated with His-tagged proteins for 8 h at 4 °C under rotation. Beads were washed with GST-binding buffer (100 mM NaCl, 50 mM NaF, 2 mM EDTA, 1% NP-40 and protease inhibitor mixture), and proteins were eluted, followed by immunoblotting.

In vitro modification assays

For the Neddylation assay, 0.25 μg of GST-RRP9, 0.5 μg of His-Smurf1 were incubated with 2 μg of Nedd8, 20 ng of E1 (APPBP1-UBA3), and 200 ng of E2 (Ubc12) in a total reaction volume of 20 μl Nedd8 conjugation Rxn Buffer Kit (BostonBiochem, SK-20). Nedd8 (UL-812), Nedd8 E1 (APPBP1/UBA3) (E-313), Ubc12 (A-655) were purchased from BostonBiochem. Samples were incubated at 30 °C for 1 h, and reactions were terminated with SDS-PAGE loading buffer before western blot.

Fluorescence microscopy

After fixation with 4% paraformaldehyde and permeabilization in 0.2% Triton X-100 (PBS), cells were incubated with the indicated antibodies for 12 h at 4 °C, followed by incubation with goat anti-rabbit IgG H&L Alexa Fluor 488 or 594 antibody for 1 h at 37 °C. The nuclei were stained with DAPI, and images were visualized with a Zeiss LSM 510 Meta inverted confocal microscope.

Generation of knockout cells

The knockout cell lines were generated using the Crispr-Cas9 method. Crispr guide sequences targeting *UBA3*, *Ubc12*, and *NEDP1* were designed by software at <http://crispr.mit.edu> and cloned into lenti-Crispr pXPR_001. The sgRNA sequences were listed in Table S1. RRP9 CRISPR/Cas9 KO plasmid was purchased from Santa Cruz (sc-411247). Smurf1 CRISPR/Cas9 KO plasmid was purchased from Santa Cruz (sc-429210). HCT116 cells were cotransfected with the lenti-

Smurf1 catalyzes RRP9 neddylation to promote tumorigenesis

Crispr vector and packaging plasmids pVSVg and psPAX2. Puromycin-resistant single cells were plated in a 96-well dish to screen for positive monoclonal cells.

Real-time PCR

Total RNA was isolated and converted to cDNA using the ReverTra Ace (Toyobo, TRT-101). Quantitative PCR reactions were carried out using SYBR Green PCR master mix (Toyobo, QPK201). Primers were shown in Table S1.

Silver staining assay

Cells were seeded onto 6-well plate petri-dishes and were then fixed in a 3:1 ethanol–acetic acid solution overnight. Cells were stained with 0.1% formic acid–50% silver nitrate solution for 5 min. Image J was used to perform NORs quantitative analysis.

β -Galactosidase, β -GAL

Cells were cultured in a 6-well plate petri-dishes and were washed twice with PBS, then were fixed for 15 min at room temperature using the stationary liquid of Staining kit (C0602; Beyotime) followed by washing for three times using PBS. Cells were then stained for 12 h at 37 °C using staining solution. After staining, cells were placed under the inverted microscope to observe the ratio of positive cells in the total cells.

Labeling of nascent RNA

The cells were cultured for 1 h in cell medium containing 1 mg/ml biotin-16-UTP. Total RNA was separated on a denaturing 1% agarose gel and then transferred to Hybond-N Hybond-NX Nylon membranes. Then labeled RNA was visualized by fluorography.

Formaldehyde-agarose gel electrophoresis

Total RNA was isolated with TRIzol according to the standard manufacturer's protocol from wild-type HCT116 cells and RRP9 knockdown cells. The RNA was added to the loading buffer before heating it at 65 °C for 5 min. Sample volumes corresponding to 10 μ g RNA were analyzed on 1% formaldehyde-agarose gel stained with ethidium bromide.

CCK8 assay

Cell proliferation was measured by the Cell Counting Kit-8 (Bimake). Cells were inoculated in 96-well plates (2 \times 10³ cells per well) and placed in the incubator (37 °C, 5%, CO₂) for an appropriate time. CCK8 was added into the 96-well plate and put in the cell culture chamber for 1 h, then the absorbance at 450 nm was measured by the enzyme reader (Molecular Devices).

Invasion assay

The 24-well plate was divided into upper end and lower end by 8 μ m polyethylene terephthalate membrane filters (Falcon). Cells were plated in serum-free DMEM medium (2 \times 10⁴ cells

per well), and DMEM medium containing 10% FBS was put in the lower end. Next, the 24-well plate was put in the incubator for 36 h. The plate was washed by PBS, fixed with 4% paraformaldehyde, and stained with 0.1% crystal violet and photographed.

Clone formation assay

The cells were seeded in 6-well plates (3 \times 10³ cells per well). Then the medium was discarded after 14 days and fixed with 4% paraformaldehyde. After staining with 1% crystal violet, photos were taken and analyzed by Image J.

Tumor growth in mice

BALB/c nude mice (6 weeks old, 18.0 \pm 2.0 g) were obtained from Shanghai Laboratory Animal Center (SLAC). Cells (5 \times 10⁶ per mouse) were inoculated subcutaneously into the right flank of the mice. Tumor size was measured every 3 days and converted to TV according to the following formula: TV (mm³) = (a \times b²)/2, where *a* and *b* are the largest and smallest diameters, respectively.

Cohort and immunohistochemistry

The colon tissue microarrays were purchased from Shanghai Biochip Company (HCol-Ade090PG, HCo-IA030PG05). The patient's pathological information was shown in Table S3. All staining was assessed by a quantitative imaging method; the percentage of immunostaining and the staining intensity were recorded. An H-score was calculated using the following formula: H-score = Σ (PI \times I) = (percentage of cells of weak intensity \times 1) + (percentage of cells of moderate intensity \times 2) + (percentage of cells of strong intensity \times 3). PI indicates the percentage of positive cells *versus* all cells.

Ethics statement

All animals were handled in strict accordance to the "Guide for the Care and Use of Laboratory Animals" and the "Principles for the Utilization and Care of Vertebrate Animals," and all animal work was approved by the Institutional Animal Care and Use Committee (IACUC) at the Capital Medical University. The colon tissue microarrays were purchased from Shanghai Biochip Company (HCol-Ade090PG, HCo-IA030PG05). Informed consent was obtained from all subjects or their relatives, and the related research was conducted in accordance with the Helsinki Declaration

Statistical analysis

Data were processed using GraphPad Prism5 (GraphPad Software). The mean \pm S.D. was from at least three independent experimental results. Student's *t* test was used to compare the two means. A *p*-value < 0.05 was considered statistically significant. **p* < 0.05, ***p* < 0.01, ****p* < 0.001, ns means "not significant."

Data availability

For IP-MS, all raw data and search results have been deposited to the PRIDE database (<http://www.iprox.org/index>) with the accession number: PXD024476 (Table S2). The authors declare that all the relevant data supporting the findings of this study are available within the article and its supporting information files or from the corresponding author on reasonable request.

Supporting information—This article contains supporting information.

Acknowledgments—This study was supported by National Natural Science Foundation of China (31971229, 81802764), National Outstanding Youth Science Fund Project of National Natural Science Foundation of China (82122052), Open Project Program of the State Key Laboratory of Proteomics (SKLP-O201901), Beijing excellent talents training project and Beijing Municipal Natural Science Foundation (7212038).

Author contributions—P. X. conceptualization; M. D., F. L., S. T., and P. X. data curation; M. D., F. L., Y. C., and P. X. formal analysis; P. X. funding acquisition; P. X. investigation; M. D., F. L., S. T., W. L., Y.-j. C., and P. X. methodology; P. X. project administration; M. D., F. L., and P. X. resources; M. D., F. L., S. T., W. L., Y.-j. C., and P. X. software; P. X. supervision; P. X. validation; P. X. visualization; M. D. and P. X. writing—original draft; Y. C. and P. X. writing—review and editing.

Conflict of interest—The authors declare that they have no conflicts of interest with the contents of this article.

Abbreviations—The abbreviations used are: C-CBL, casitas B-lineage lymphoma c; CSN5, COP9 signalosome subunit 5; DCN1, defective in cullin neddylation protein; KI, knock-in; KO, knockout; MDM2, mouse double minute 2; MEKK2, mitogen-activated protein kinase kinase kinase 2; NAE1, NEDD8 activating enzyme E1 subunit 1; NEDP1, nedd8 protease 1; PCAF, P300/CBP-associated factor; PTEN, gene of phosphate and tension homology deleted on chromosome ten; RBX1, ring-box 1; RNF111, ring finger protein 111; RNF168, ring finger protein 168; RRP9, ribosomal RNA processing 9; SIRT7, sirtuin 7; UBA3, ubiquitin-like modifier activating enzyme 3; UBE2F, ubiquitin conjugating enzyme E2 F; UBE2M, ubiquitin conjugating enzyme E2 M; XIAP, X-linked inhibitor of apoptosis.

References

- Henras, A. K., Soudet, J., Gerus, M., Lebaron, S., Caizergues-Ferrer, M., Mougin, A., and Henry, Y. (2008) The post-transcriptional steps of eukaryotic ribosome biogenesis. *Cell Mol. Life Sci.* **65**, 2334–2359
- Tafforeau, L., Zorbas, C., Langhendries, J. L., Mullineux, S. T., Stamato-poulou, V., Mullier, R., Wacheul, L., and Lafontaine, D. L. (2013) The complexity of human ribosome biogenesis revealed by systematic nuclear screening of Pre-rRNA processing factors. *Mol. Cell* **51**, 539–551
- Lafontaine, D. L. (2015) Noncoding RNAs in eukaryotic ribosome biogenesis and function. *Nat. Struct. Mol. Biol.* **22**, 11–19
- Baßler, J., and Hurt, E. (2019) Eukaryotic ribosome assembly. *Annu. Rev. Biochem.* **88**, 281–306
- Ojha, S., Malla, S., and Lyons, S. M. (2020) snoRNPs: Functions in ribosome biogenesis. *Biomolecules* **10**, 783
- François, D., Jennifer, G., Patricia, A., Brianna, M., Kara, P., Karen, W., Steven, W., Robert, S., Jeffrey, S., Yvonne, O., Ann, B., Donald, H., and Susan, B. (2000) A large nucleolar U3 ribonucleoprotein required for 18S ribosomal RNA biogenesis. *Nature* **417**, 967–970
- Kass, S., Tyc, K., Steitz, J. A., and Sollner-Webb, B. (1990) The U3 small nucleolar ribonucleoprotein functions in the first step of preribosomal RNA processing. *Cell* **60**, 897–908
- Aittaleb, M., Rashid, R., Chen, Q., Palmer, J. R., Daniels, C. J., and Li, H. (2003) Structure and function of archaeal box C/D sRNP core proteins. *Nat. Struct. Biol.* **10**, 256–263
- Beltrame, M., and Tollervey, D. (1995) Base pairing between U3 and the pre-ribosomal RNA is required for 18S rRNA synthesis. *EMBO J.* **14**, 4350–4356
- Choudhary, C., Kumar, C., Gnad, F., Nielsen, M. L., Rehman, M., Walther, T. C., Olsen, J. V., and Mann, M. (2009) Lysine acetylation targets protein complexes and co-regulates major cellular functions. *Science* **325**, 834–840
- Chen, S., Blank, M. F., Iyer, A., Huang, B., Wang, L., Grummt, I., and Voit, R. (2016) SIRT7-dependent deacetylation of the U3-55k protein controls pre-rRNA processing. *Nat. Commun.* **7**, 10734
- Kerscher, O., Felberbaum, R., and Hochstrasser, M. (2006) Modification of proteins by ubiquitin and ubiquitin-like proteins. *Annu. Rev. Cell Dev. Biol.* **22**, 159–180
- Enchev, R. I., Schulman, B. A., and Peter, M. (2015) Protein neddylation: Beyond cullin-RING ligases. *Nat. Rev. Mol. Cell Biol.* **16**, 30–44
- Mendoza, H. M., Shen, L. N., Botting, C., Lewis, A., Chen, J., Ink, B., and Hay, R. T. (2003) NEDP1, a highly conserved cysteine protease that deNEDDylates cullins. *J. Biol. Chem.* **278**, 25637–25643
- Cope, G. A., Suh, G. S., Aravind, L., Schwarz, S. E., Zipursky, S. L., Koonin, E. V., and Deshaies, R. J. (2002) Role of predicted metalloprotease motif of Jab1/Csn5 in cleavage of Nedd8 from Cul1. *Science* **298**, 608–611
- Soucy, T. A., Smith, P. G., Milhollen, M. A., Berger, A. J., Gavin, J. M., Adhikari, S., Brownell, J. E., Burke, K. E., Cardin, D. P., Critchley, S., Cullis, C. A., Doucette, A., Garnsey, J. J., Gaulin, J. L., Gershman, R. E., et al. (2009) An inhibitor of NEDD8-activating enzyme as a new approach to treat cancer. *Nature* **458**, 732–736
- Yoshimura, C., Muraoka, H., Ochiwa, H., Tsuji, S., Hashimoto, A., Kazuno, H., Nakagawa, F., Komiya, Y., Suzuki, S., Takenaka, T., Kumazaki, M., Fujita, N., Mizutani, T., and Ohkubo, S. (2019) TAS4464, a highly potent and selective inhibitor of NEDD8-activating enzyme, suppresses neddylation and shows antitumor activity in diverse cancer models. *Mol. Cancer Ther.* **18**, 1205–1216
- Zhou, L., and Jia, L. (2020) Targeting protein neddylation for cancer therapy. *Adv. Exp. Med. Biol.* **1217**, 297–315
- Mao, H., and Sun, Y. (2020) Neddylation-independent activities of MLN4924. *Adv. Exp. Med. Biol.* **1217**, 363–372
- Zhou, L., Jiang, Y., Luo, Q., Li, L., and Jia, L. (2019) Neddylation: A novel modulator of the tumor microenvironment. *Mol. Cancer* **18**, 77
- Huang, D. T., Walden, H., Duda, D., and Schulman, B. A. (2004) Ubiquitin-like protein activation. *Oncogene* **23**, 1958–1971
- Kamura, T., Conrad, M. N., Yan, Q., Conaway, R. C., and Conaway, J. W. (1999) The Rbx1 subunit of SCF and VHL E3 ubiquitin ligase activates Rub1 modification of cullins Cdc53 and Cul2. *Genes Dev.* **13**, 2928–2933
- Kurz, T., Chou, Y. C., Willems, A. R., Meyer-Schaller, N., Hecht, M. L., Tyers, M., Peter, M., and Sicheri, F. (2008) Dcn1 functions as a scaffold-type E3 ligase for cullin neddylation. *Mol. Cell* **29**, 23–35
- Xirodimas, D. P., Saville, M. K., Bourdon, J. C., Hay, R. T., and Lane, D. P. (2004) Mdm2-mediated NEDD8 conjugation of p53 inhibits its transcriptional activity. *Cell* **118**, 83–97
- Yang, X., Zhou, J., Sun, L., Wei, Z., Gao, J., Gong, W., Xu, R., Rao, Z., and Liu, Y. (2007) Structural basis for the function of DCN-1 in protein neddylation. *J. Biol. Chem.* **282**, 24490–24494
- Benjamin, S., and Steller, H. (2010) Another tier for caspase regulation: IAPs as NEDD8 E3 ligases. *Dev. Cell* **19**, 791–792
- Ma, T., Chen, Y., Zhang, F., Yang, C. Y., Wang, S., and Yu, X. (2013) RNF111-dependent neddylation activates DNA damage-induced ubiquitination. *Mol. Cell* **49**, 897–907
- Li, T., Guan, J., Huang, Z., Hu, X., and Zheng, X. (2014) RNF168-mediated H2A neddylation antagonizes ubiquitylation of H2A and regulates DNA damage repair. *J. Cell Sci.* **127**, 2238–2248

Smurf1 catalyzes RRP9 neddylation to promote tumorigenesis

29. Xie, P., Zhang, M., He, S., Lu, K., Chen, Y., Xing, G., Lu, Y., Liu, P., Li, Y., Wang, S., Chai, N., Wu, J., Deng, H., Wang, H. R., Cao, Y., *et al.* (2014) The covalent modifier Nedd8 is critical for the activation of Smurf1 ubiquitin ligase in tumorigenesis. *Nat. Commun.* **5**, 3733
30. Li, H., Zhu, H., Liu, Y., He, F., Xie, P., and Zhang, L. (2016) Itch promotes the neddylation of JunB and regulates JunB-dependent transcription. *Cell Signal* **28**, 1186–1195
31. Zhu, H., Kavsak, P., Abdollah, S., Wrana, J. L., and Thomsen, G. H. (1999) A SMAD ubiquitin ligase targets the BMP pathway and affects embryonic pattern formation. *Nature* **400**, 687–693
32. Yamashita, M., Ying, S. X., Zhang, G. M., Li, C., Cheng, S. Y., Deng, C. X., and Zhang, Y. E. (2005) Ubiquitin ligase Smurf1 controls osteoblast activity and bone homeostasis by targeting MEKK2 for degradation. *Cell* **121**, 101–113
33. Narimatsu, M., Bose, R., Pye, M., Zhang, L., Miller, B., Ching, P., Sakuma, R., Luga, V., Roncari, L., Attisano, L., and Wrana, J. L. (2009) Regulation of planar cell polarity by Smurf ubiquitin ligases. *Cell* **137**, 295–307
34. Cao, Y., and Zhang, L. (2013) A Smurf1 tale: Function and regulation of an ubiquitin ligase in multiple cellular networks. *Cell Mol. Life Sci.* **70**, 2305–2317
35. Barrios-Rodiles, M., Brown, K. R., Ozdamar, B., Bose, R., Liu, Z., Donovan, R. S., Shinjo, F., Liu, Y., Dembowy, J., Taylor, I. W., Luga, V., Przulj, N., Robinson, M., Suzuki, H., Hayashizaki, Y., *et al.* (2005) High-throughput mapping of a dynamic signaling network in mammalian cells. *Science* **307**, 1621–1625
36. Newman, D. R., Kuhn, J. F., Shanab, G. M., and Maxwell, E. S. (2000) Box C/D snoRNA-associated proteins: Two pairs of evolutionarily ancient proteins and possible links to replication and transcription. *RNA* **6**, 861–879
37. Rothé, B., Manival, X., Rolland, N., Charron, C., Senty-Ségault, V., Branlant, C., and Charpentier, B. (2017) Implication of the box C/D snoRNP assembly factor Rsa1p in U3 snoRNP assembly. *Nucleic Acids Res.* **45**, 7455–7473
38. Pelletier, J., Thomas, G., and Volarevic, S. (2018) Ribosome biogenesis in cancer: New players and therapeutic avenues. *Nat. Rev. Cancer* **18**, 51–63
39. Kampen, K. R., Sulima, S. O., Vereecke, S., and Keersmaecker, K. D. (2020) Hallmarks of ribosomopathies. *Nucleic Acids Res.* **48**, 1013–1028
40. He, S., Cao, Y., Xie, P., Dong, G., and Zhang, L. (2017) The Nedd8 non-covalent binding region in the Smurf HECT domain is critical to its ubiquitin ligase function. *Sci. Rep.* **7**, 41364
41. Xia, Q., Zhang, H., Zhang, P., Li, Y., Xu, M., Li, X., and Dong, L. (2020) Oncogenic Smurf1 promotes PTEN wild-type glioblastoma growth by mediating PTEN ubiquitylation. *Oncogene* **39**, 5902–5915
42. Xie, P., Peng, Z., Chen, Y., Li, H., Du, M., Tan, Y., Zhang, X., Lu, Z., Cui, C. P., Liu, C. H., He, F., and Zhang, L. (2021) Neddylation of PTEN regulates its nuclear import and promotes tumor development. *Cell Res.* **31**, 291–311
43. Qian, G., Hu, X., Li, G., Ding, Y., Zhu, L., and Zheng, H. (2018) Smurf1 restricts the antiviral function mediated by USP25 through promoting its ubiquitination and degradation. *Biochem. Biophys. Res. Commun.* **498**, 537–543
44. Feng, X., Jia, Y., Zhang, Y., Ma, F., Zhu, Y., Hong, X., Li, M., Li, Z., Pan, J., Li, Y., Li, G., Yang, C., Liu, Y., Xie, Y., and Lv, H. (2019) Ubiquitination of UVRAG by SMURF1 promotes autophagosome maturation and inhibits hepatocellular carcinoma growth. *Autophagy* **15**, 1130–1149
45. Zhang, L., Lin, J., and Ye, K. (2013) Structural and functional analysis of the U3 snoRNA binding protein Rrp9. *RNA* **19**, 701–711
46. Venema, J., Vos, H. R., Faber, A. W., van Venrooij, W. J., and Raué, H. A. (2000) Yeast Rrp9p is an evolutionarily conserved U3 snoRNP protein essential for early pre-rRNA processing cleavages and requires box C for its association. *RNA* **6**, 1660–1671
47. Lukowiak, A. A., Granneman, S., Mattox, S. A., Speckmann, W. A., Jones, K., Pluk, H., Venrooij, W. J., Terns, R. M., and Terns, M. P. (2000) Interaction of the U3-55k protein with U3 snoRNA is mediated by the box B/C motif of U3 and the WD repeats of U3-55k. *Nucleic Acids Res.* **28**, 3462–3471